REPORT DOCUMENTATION PAGE

Public reporting burden for this collection of information is estimated to average 1 hour per response, including the time for reviewing instructions, searching existing data sources, gathering and maintaining the data needed, and completing and reviewing the collection of information. Send comments regarding this burden estimate or any other aspect of this collection of information, including suggestions for reducing this burden to Washington Headquarters Services, Directorate for Information Operations and Reports, 1215 Jefferson Davis Highway, Suite 1204, Arlington, VA 22202-4302, and to the Office of Management and Budget, Paperwork Reduction Project (0704-0188), Washington, DC 20503.

PLEASE DO NOT RETURN YOUR FORM TO THE ABOVE ADDRESS.

1. REPORT DATE (DD-MM-YYYY)	2. REPORT TYPE	3. DATES COVERED
	Journal Article	

4. TITLE AND SUBTITLE

The Impact of Water Turbidity on Interannual Sea Surface Temperature Simulation in a Layered Global Ocean Model

5a. CONTRACT NUMBER

5b. GRANT NUMBER

5c. PROGRAM ELEMENT NUMBER

601153N

6. AUTHOR(S)

A. Birol Kara, Harley E. Hurlburt and Peter A. Rochford

5d. PROJECT NUMBER

5e. TASK NUMBER

5f. WORK UNIT NUMBER

7. PERFORMING ORGANIZATION NAME(S) AND ADDRESS(ES)
Naval Research Laboratory
Oceanography Division
Stennis Space Center, MS 39529-5004

8. PERFORMING ORGANIZATION REPORT NUMBER

NRL/JA/7304/02/0002

9. SPONSORING/MONITORING AGENCY NAME(S) AND ADDRESS(ES)
Office of Naval Research
800 N. Quincy St.
Arlington, VA 22217-5660

10. SPONSOR/MONITOR'S ACRONYM(S)

ONR

11. SPONSOR/MONITOR'S REPORT NUMBER(S)

12. DISTRIBUTION/AILABILITY STATEMENT

Approved for public release; distribution is unlimited

13. SUPPLEMENTARY NOTES

20040604 116

14. ABSTRACT

The Naval Research Laboratory (NRL) Layered Ocean Model (NLOM) with an embedded bulk-type mixed layer model is used to examine the effects of ocean turbidity on sea surface temperature (SST) and ocean mixed layer depth (MLD) simulations over the global ocean. The model accounts for ocean turbidity through depth-dependent attenuation of solar radiation in the mixed layer formulation as determined from the diffusive attenuation coefficient at 490 nm ($k4,\sim$) obtained by the Sea-Viewing Wide Field-of-View Sensor (ScaW1FS). Interannual model simulations are used to assess the first-order effects of ocean turbidity on SST and MLD simulation. Results are reported from three model experiments performed using different values for the attenuation of photosynthetically available radiation ($k\sim\sim$). It is shown that, although allowing incoming solar radiation to vary in time and space is desirable for predicting SST, in an OGCM use of a constant $\sim$ with a value of 0.06 m' is generally sufficient in the deep ocean. The daily averaged SST time series from the three NLOM simulations are verified against daily in situ SSTs reported from 12 moored buoys in 1996 and 1999.

15. SUBJECT TERMS
turbidity, sea surface temperature, layered global ocean mode

16. SECURITY CLASSIFICATION OF:			17. LIMITATION OF ABSTRACT	18. NUMBER OF PAGES	19a. NAME OF RESPONSIBLE PERSON
a. REPORT	b. ABSTRACT	c. THIS PAGE			Harley Hurlburt
Unclassified	Unclassified	Unclassified	SAR	14	19b. TELEPHONE NUMBER (Include area code)
					228-688-4626

The Impact of Water Turbidity on Interannual Sea Surface Temperature Simulations in a Layered Global Ocean Model*

A. BIROL KARA, HARLEY E. HURLBURT, AND PETER A. ROCHFORD[+]

Naval Research Laboratory, Stennis Space Center, Mississippi

JAMES J. O'BRIEN

Center for Ocean–Atmospheric Prediction Studies, The Florida State University, Tallahassee, Florida

ABSTRACT

The Naval Research Laboratory (NRL) Layered Ocean Model (NLOM) with an embedded bulk-type mixed layer model is used to examine the effects of ocean turbidity on sea surface temperature (SST) and ocean mixed layer depth (MLD) simulations over the global ocean. The model accounts for ocean turbidity through depth-dependent attenuation of solar radiation in the mixed layer formulation as determined from the diffusive attenuation coefficient at 490 nm (k_{490}) obtained by the Sea-Viewing Wide Field-of-View Sensor (SeaWiFS). Interannual model simulations are used to assess the first-order effects of ocean turbidity on SST and MLD simulation. Results are reported from three model experiments performed using different values for the attenuation of photosynthetically available radiation (k_{PAR}). It is shown that, although allowing incoming solar radiation to vary in time and space is desirable for predicting SST, in an OGCM use of a constant k_{PAR} with a value of 0.06 m^{-1} is generally sufficient in the deep ocean. The daily averaged SST time series from the three NLOM simulations are verified against daily in situ SSTs reported from 12 moored buoys in 1996 and 1997. Model results show that allowing the possibility of solar heating below the mixed layer reduces the root-mean-square error (rmse) difference between the daily yearlong model and buoy SST time series by up to 0.4°C and reduces the rmse at 11 of the 12 buoy locations. Although using spatially and temporally varying k_{PAR} versus a constant $k_{PAR} = 0.06$ m^{-1} (which is representative over most of the global ocean) had low impact overall, using it generally reduced the rmse at low latitudes, and using it can have a substantial impact locally in space and time. The model MLD results show low sensitivity to the k_{PAR} value used.

1. Introduction

Ocean mixed layer models play an important role in simulated air–sea interactions and are required to explain upper-ocean characteristics (e.g., Martin 1985; Sterl and Kattenberg 1994; Schopf and Loughe 1995). The major difficulty in parameterizing the ocean mixed layer is that the ocean boundary layer is not as fully observed as the atmospheric boundary layer (e.g., Smith et al. 1996). Thus, specific attention must be given to the atmospheric forcing that drives the upper ocean.

Sensible and latent heat fluxes, longwave and shortwave radiation, wind stress, and ocean surface temperature constitute the principal means for coupling between the atmosphere and ocean. Among these variables, the vertical distribution of shortwave radiation within the ocean is significant for upper-ocean studies because radiation can penetrate below the mixed layer and destabilize the stratification (e.g., Austin and Petzold 1986; Morel and Antonie 1994; Morel and Maritonera 2001), thereby affecting SST during upwelling/downwelling events (Nakamoto et al. 2000). Knowledge of the shortwave radiation within the ocean is particularly critical for understanding dynamical and thermodynamical processes occurring in the ocean surface mixed layer. For example, the amount of solar irradiance affects sea surface temperature (SST) and ocean surface mixed layer depth (MLD) by changing the surface energy budget of the water (e.g., Gallimore and Houghton 1987; Lewis et al. 1990), and it controls the rates of photosynthetic processes (e.g., Frouin et al. 1989; Brock and McClain 1992; Brock et al. 1993). We note here that unlike the atmospheric boundary layer, which is nearly transparent, the ocean boundary layer strongly absorbs solar radiation. Thus, changes in upper-ocean

Corresponding author address: Birol Kara, Naval Research Laboratory, Code 7323, Bldg. 1009, Stennis Space Center, MS 39529-5004.
E-mail: kara@nrlssc.navy.mil

characteristics are closely tied to variations in solar radiation within the ocean and its attenuation within the water column, which need to be taken into account in numerical ocean modeling studies. Radiation attenuation might also be significant for long-term climate variability if the attenuation depth scale is greater than the MLD. For example, a fraction of the solar radiation heating might be absorbed below the thermocline during the onset of an El Niño event (e.g., Woods 1994). This heating may not be redistributed easily by the mixed layer and could be significant on interannual time scales.

Bulk mixed layer models (e.g., Garwood 1977; Niller and Kraus 1977; Price et al. 1986) and diffusion-based mixed layer models (e.g., Mellor and Yamada 1982) have different responses to solar heating as reviewed by Kantha and Clayson (1994). The sensitivity to the distribution of the solar radiation (Simpson and Dickey 1981; Dickey 1983; Le Treut et al. 1985) is primarily because vertical stratification plays a controlling role in the vertical turbulent mixing. As was shown in Simonot and Le Treut (1986), part of the solar radiation can be absorbed below the MLD at low latitudes. Therefore, the modification of the water optical properties can change the density field of the ocean and the dynamical response of the oceanic layers to surface wind stress forcing (e.g., Kara et al. 2000a). High turbidity also raises the temperature in a shallow mixed layer, thus changing the SST and stratification. This implies that a good representation of optical properties of seawater is necessary for accurate modeling of SST and MLD. The importance of solar extinction in the upper ocean in relation to the diurnal cycle was discussed using a mixed layer model based on second-moment closure of turbulence (Kantha and Clayson 1994). They explained that the rise in SST for a very shallow MLD is highly sensitive to the parameterization of the solar extinction that includes different Jerlov (1976, 1977) water types. When using a clear water type instead of a variable water type in their simulations, the diurnal cycle of SST essentially disappeared. Other studies (e.g., Woods et al. 1984; Lewis et al. 1990) have also discussed the effects of optical water types on the ocean surface mixed layer. They indicated the need to consider the penetration of solar irradiance in developing simulations of tropical Pacific SST.

The sensitivity of SST and MLD evolution to solar transmission in large-scale ocean general circulation model (OGCM) studies has also been investigated. For example, Schneider and Zhu (1998) showed with a coupled atmosphere–ocean GCM that inclusion of sunlight penetration was essential to correctly simulate the strong semiannual SST cycle in the eastern equatorial Pacific. This was achieved using a constant penetration depth of 15 m and did not use any satellite-based ocean color data to account for water turbidity. Murtugudde et al. (2002) illustrated the importance of a realistic treatment of penetrating radiation in climate models by using spatially varying annual-mean attenuation depths that were

estimated from remotely sensed chlorophyll concentrations provided by the Coastal Zone Color Scanner (CZCS). While their OGCM study was limited to the Tropics because of the available coverage of CZCS, the study did show significant improvement in model SST simulations when using annual-mean attenuation depths versus a constant value of 17 m. The study by Nakamoto et al. (2001) examined the effects of including space- and time-varying solar attenuation with depth by using monthly CZCS chlorophyll concentrations where available over the World Ocean. Their analysis of the model simulations focused on the equatorial Pacific. Ohlmann et al. (1996) used monthly CZCS data with a fully spectral radiation model to show that solar radiation penetration can be a significant term in the mixed layer heat budget for the tropical regions. Rochford et al. (2001) constructed a global monthly mean climatology for the attenuation of photosynthetically available radiation (PAR), denoted as k_{PAR}, using a diffusive attenuation coefficient at 490 nm (k_{490}). They showed that the inclusion of solar subsurface heating is important for improving the global OGCM simulation of SST in the equatorial regions, while subsurface heating is not important for MLD simulations. Although these studies indicate the importance of including a penetrating radiation scheme to improve model SST and MLD simulations, none examined the effects of water turbidity on SST and MLD simulations on short time scales (e.g., daily).

The main goal of this paper is to indicate the regions where water turbidity variability can affect SST and MLD simulations over the global ocean on daily time scales. For this purpose we examine daily SST and MLD sensitivity to subsurface heating using interannual simulations from the Naval Research Laboratory (NRL) Layered Ocean Model (NLOM) with an embedded mixed layer. All model simulations presented in this paper use atmospheric forcing with high temporal (6 hourly) resolution. Model–data comparisons are performed using daily moored buoy observations.

This paper is organized as follows. In section 2, a brief description is given of the NLOM mixed layer implementation, surface forcing, turbulence model, and model parameterizations. In section 3, the effects of ocean turbidity on the model simulations are explained by comparing the daily model SST time series with daily buoy SST time series over the different regions of the global ocean. Some comparisons are also made between the findings obtained from NLOM and the findings of similar studies that used different OGCMs. A summary and conclusions of this paper are presented in section 4.

2. Mixed layer model description

The numerical ocean model used is a primitive equation layered formulation in which the equations have been vertically integrated through each layer. The NLOM is a descendent of the model by Hurlburt and
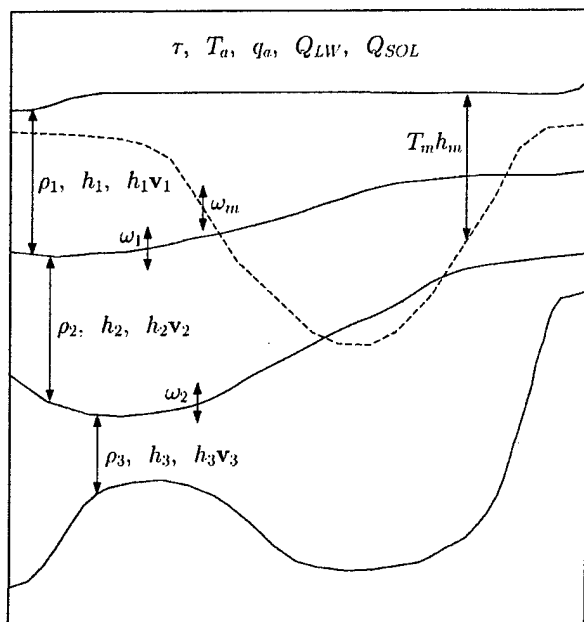
FIG. 1. Schematic illustration of mixed layer structure in the NLOM adapted from Wallcraft et al. (2003). For simplicity, only three thermodynamic layers and the mixed layer are shown, although six layers plus the mixed layer are used in this study. Prognostic variables are layer density (ρ_k), layer thickness (h_k), layer transport per unit width $(h_k v_k)$, mixed layer temperature (T_m), and MLD (h_m). Atmospheric forcing is wind stress (τ), air temperature (T_a), mixing ratio at 10 m above the sea surface (q_a), longwave radiation (Q_{LW}), and downward solar irradiance at the sea surface (Q_{SOL}).

Thompson (1980) with enhancements by Wallcraft (1991), Wallcraft and Moore (1997), and Moore and Wallcraft (1998). It can be run in reduced-gravity mode, in which the lowest layer is infinitely deep and at rest, or in finite-depth mode, which allows realistic bottom topography. In addition, NLOM can be run in hydrodynamic mode (spatially and temporally constant density within each layer; e.g., Hurlburt et al. 1996) or in thermodynamic mode (spatially and temporally varying density within each layer—i.e., density is a prognostic variable; e.g., Metzger and Hurlburt 2001). The model boundary conditions are kinematic and no slip. Prognostic variables are layer density, layer thickness, and layer volume transport. The model includes entrainment (detrainment) processes by allowing the exchange of mass, momentum, and heat between the layers.

The model domain used for this study covers the global ocean from 72°S to 65°N, gridded to a resolution of 0.5° in latitude and 0.703 125° in longitude. The lateral boundaries follow the 200-m isobath. One of the major advantages of NLOM over other types of OGCMs such as z-level and sigma-coordinate models is its lower computational cost for the same model domain and horizontal resolution. One reason is that we can use lower vertical resolution to realistically represent the ocean circulation. For example, in the (½°) model there are

only six dynamical layers plus a semipassive mixed layer in the vertical with layer thickness that varies in both time and space. NLOM is also a single efficient portable and scalable computer code that can run any of the model configurations on a variety of computing platforms (Wallcraft and Moore 1997).

In this paper, we give only a brief description of the embedded mixed layer parameterizations. See Wallcraft et al. (2003) for a full description of the model formulations and the ½° global model used here. See Kara et al. (2000b, 2002a) for the parameterizations used in calculating atmospheric forcing fields.

a. Mixed layer equations

The NLOM has typically been run without an explicit mixed layer, which is equivalent to assuming the mixed layer is always inside the upper layer, but now the model has been extended with an "almost passive" embedded well-mixed surface turbulent boundary layer. A schematic illustration of the global NLOM with an embedded mixed layer is shown in Fig. 1.

The embedded mixed layer model employed here carries prognostic equations for the SST (T_m) and MLD (h_m) as follows;

SST:

$$\frac{\partial T_m}{\partial t} + \mathbf{v}_1 \cdot \nabla T_m = -\frac{\max(0, \omega_m)}{h_m}(T_m - \Delta T_m - T_b)$$

$$+ \frac{Q_a - Q_P e^{-h_m/h_P}}{\rho_0 C_{pa} h_m} + \frac{K_H}{h_m}\nabla \cdot (h_m \nabla T_m)$$

$$(1)$$

MLD:

$$\frac{\partial (h_m)}{\partial t} + \nabla \cdot (h_m \mathbf{v}_1) = \omega_m. \qquad (2)$$

The symbols appearing in the equations are defined in the appendix along with their units. Major free parameters in Eqs. (1) and (2) are net surface heat flux (Q_a), temperature shear at the base of the mixed layer $[\Delta T_b = (T_m - \Delta T_m) - T_b]$, and vertical mixing velocity (ω_m). These free parameters are obtained from a surface energy budget (section 2b) and from a continuous model temperature profile, respectively. The temperature change across the mixed layer is ΔT_m, specified as a function of latitude based on the NMLD monthly climatology (Kara et al. 2002b). The values of ΔT_m range from 0.1°C at high latitudes to 1.5°C at low latitudes.

In the model simulations, the Laplacian temperature diffusion in Eq. (1) is typically turned off (i.e., $K_H = 0$) because the van Leer monotonic scheme (Lin et al. 1994) used for advection contributes sufficient nonlinear diffusion for stability. This scheme allows NLOM to be run using a very small minimum imposed MLD (e.g., 10 m).

b. Surface energy balance

The net surface heat flux that has been absorbed (or lost) by the upper ocean to depth z, $Q(z)$, is parameterized as the sum of the downward surface solar irradiance (Q_{SOL}), upward longwave radiation (Q_{LW}), and the downward latent and sensible heat fluxes (Q_L and Q_S, respectively). The solar irradiance at the ocean surface ranges in wavelength from about 300 to 2800 nm and is composed of three general regions: the ultraviolet (UV) below 400 nm, the visible at 400–700 nm, and the infrared (IR) above 700 nm. The light available for photosynthesis by photoplankton is the PAR and is defined as the 350–700-nm range of the spectrum (e.g., Liu et al. 1994). It accounts for 43%–50% of the solar irradiance at the sea surface (Rochford et al. 2001).

For the NLOM surface forcing, the surface solar irradiance is decomposed into its infrared (Q_{IR}) and penetrating radiation (Q_P) as $Q_{SOL} = Q_{IR} + Q_P$, thereby enabling us to write

$$Q(z) = Q_{IR} + Q_P(z) - Q_{LW} + Q_L + Q_S. \quad (3)$$

Since the Q_{IR} component is absorbed within the first few centimeters of the sea, a depth which is much less than the minimum MLD imposed in most OGCMs (10 m for the NLOM), all of the IR radiation arriving at the air–sea interface is used to heat the surface layer of the ocean model. The Q_P component for the PAR and UV portion of the spectrum that penetrates to greater depths can be well represented by a single exponential. Based on global monthly climatologies of Q_P and Q_{SOL}, $Q_{IR} = 0.49Q_{SOL}$ is assumed everywhere over the global ocean. Thus, the expression for subsurface heating is obtained as follows:

$$Q(z) = Q_a - Q_P e^{(-z/h_P)}, \quad (4)$$

$$h_P = 1/k_{PAR}, \quad \text{and} \quad (5)$$

$$Q_a = Q_{SOL} - Q_{LW} + Q_L + Q_S. \quad (6)$$

Here Q_a is the net heat flux at the ocean surface. The rate of surface heating/cooling of the mixed layer is simply obtained by evaluating this expression at the MLD (i.e., $z = h_m$), and the remaining solar radiation, $Q(h_m)$, is applied below the mixed layer. The radiation absorption length scale in Eq. (5) is expressed as $h_P = 1/k_{PAR}$.

It is noted that we use Eq. (4) although fully spectral representations are available (e.g., Morel and Maritorena 2001). In general, OGCMs that have few layers near the surface (e.g., Schneider and Zhu 1998), with a minimum MLD, for example, 10 m, use simple solar irradiance approximations, such as single or bimodal exponential parameterizations (Paulson and Simpson 1977; Zaneveld and Spinrad 1980). This is because, for depths greater than 10 m, the penetrative solar flux can be accurately determined by resolving just the 300–745-nm spectral region, which is well represented by a single exponential below 10 m.

As explained in detail in Kara et al. (2003, unpublished manuscript, hereinafter KHR), the attenuation depth for PAR differs depending on water type (Simonot and Le Treut 1986) and is quite variable over the global ocean. The extent to which PAR penetrates into and below the mixed layer has been quantified using remotely sensed satellite color data and used in other OGCM studies (e.g., Schneider and Zhu 1998; Murtugudde et al. 2002; Kara et al. 2003b). To properly include effects of turbidity, the model therefore reads in monthly k_{PAR} fields (KHR) based on Sea-Viewing Wide Field-of-View Sensor (SeaWiFS) data (McClain et al. 1998). Thus, our approach amounts to a one-band versus two-band approach, where the red and near-infrared radiation is completely absorbed within the minimum MLD of 10 m imposed by the NLOM, and the penetrating radiation portion is allowed to have space and time variations.

Latent and sensible heat fluxes at the air–sea interface are calculated using efficient and computationally inexpensive simple bulk formulas that include the effects of dynamic stability (Kara et al. 2002a). The combination of accuracy and ease of computation of this method makes it the one preferred for computing air–sea fluxes in the NLOM. Note that both sensible and latent heat fluxes are calculated using mixed layer temperature (T_m) at the model time step. Radiation flux (shortwave and longwave fluxes) is so dependent on cloudiness that this is taken directly from European Centre for Medium-Range Weather Forecasts (ECMWF) data (ECMWF 1995; Gibson et al. 1997) for use in the model. Basing fluxes on the model SST automatically provides a physically realistic tendency toward the "correct" SST. If the model SST is too high or low, the flux is reduced or increased relative to that from the correct SST. In NLOM, the accuracy of the SST is also enhanced by relaxing the dynamic layer densities below the mixed layer back toward climatology (monthly in layer 1, annually otherwise), in addition to applying the heat flux (Kara et al. 2003b). There is no direct SST relaxation term in the equation, but entrainment at the base of the mixed layer allows the dynamical layer density relaxation to influence SST.

c. Turbulence model

The rate of mixed layer deepening or retreat, ω_m, is determined using a modified version of the KT model (Kraus and Turner 1967; Niiler and Kraus 1977). This involves solving the vertically integrated turbulent kinetic energy (TKE) equation for a stationary budget. The TKE budget (P) implemented in the NLOM for the present study is already derived in KHR with particular attention to the attenuation of solar radiation with depth:

$$P = (m_3 - m_1)u_*^3$$

$$- h_m \left(\frac{n_c}{2} b_* w_* - m_6 \delta b_* w_* + m_5 \hat{f} u_*^2 \right) + B_{rad}, \quad (7)$$

where

$$u_*^2 = \frac{|\tau_a|}{\rho_0}, \tag{8}$$

$$b_* w_* = \frac{g\alpha(T_m)}{\rho_0 C_{pw}}(Q_a - Q_P), \tag{9}$$

$$\delta = \begin{cases} 1, & \text{for } b_* w_* < 0 \\ 0, & \text{for } b_* w_* \geq 0, \end{cases} \tag{10}$$

$$\hat{f} = \max(|2\Omega \sin(\phi)|, f^+), \tag{11}$$

and B_{rad} contains the contribution due to attenuation of solar radiation that will be specified further below.

When shallowing (i.e., $P < 0$), mixing occurs toward the equilibrium depth as follows:

$$h_m^* = \frac{(m_3 - m_1)u_*^3}{\dfrac{n_c}{2}b_* w_* - \dfrac{B_{\text{rad}}}{h_m} - m_6\delta b_* w_* + m_5\hat{f}u_*^2}, \quad \text{and} \tag{12}$$

$$\omega_m = \sigma_\omega[\max(h_m^*, h_m^+) - h_m]. \tag{13}$$

A relaxation time scale (σ_ω) is introduced to account for a delayed retreat of the mixed layer to the equilibrium depth. When deepening (i.e., $P > 0$), the available TKE is converted to potential energy as follows:

$$\omega_m = \frac{P}{g\alpha(T_m) \max(\Delta T_b, \Delta T_b^+)h_m}, \tag{14}$$

$$\Delta T_b = (T_m - \Delta T_m) - T_b. \tag{15}$$

A minimum value is imposed on the MLD ($h_m^+ = 10$ m) and ΔT_b represents the temperature difference at the base of the mixed layer. Since ΔT_b is not guaranteed to be positive, an alternative minimum value ($\Delta T_b^+ = 0.2°C$) is specified. For further information on the details and rationale for the above the reader is referred to Wallcraft et al. (2003).

Various possible forms can be chosen for the contribution due to radiation penetration (B_{rad}) and these can have functional dependencies upon h_m that are highly nontrivial. To retain a reasonable level of simplicity so that insight can be gained when including and excluding the effects of subsurface heating, we employ the following for B_{rad} in this study:

$$B_{\text{rad}} = -\frac{n_c}{2}h_m\frac{g\alpha}{\rho_0 C_{pw}}Q_P(1 - e^{-h_m/h_P}). \tag{16}$$

This choice reproduces the essential result for B_{rad} when h_P becomes extremely small,

$$\lim_{h_P \to 0} B_{\text{rad}} = -\frac{n_c}{2}h_m\frac{g\alpha}{\rho_0 C_{pw}}Q_P, \tag{17}$$

while capturing the maximum possible effect of the subsurface heating for finite values of h_P. As noted in KHR, the form derived for B_{rad} is strictly valid only within the surface layer, which does not necessarily extend over the entire depth of the mixed layer, and serves only to guide the choice of parameterization. With this chosen

form for B_{rad} one has the property that $B_{\text{rad}} \leq 0$ ($Q_P \geq 0$), thereby facilitating interpretation of the effects of including subsurface heating. For example, when shallowing (i.e., $P < 0$), the equilibrium depth now becomes

$$h_m^* = \frac{(m_3 - m_1)u_*^3}{\dfrac{n_c}{2}b_* u_* - m_6\delta b_* w_* + m_5\hat{f}u_*^2}, \tag{18}$$

where

$$b_* u_* = \frac{g\alpha(T_m)}{\rho_0 C_{pw}}(Q_a - Q_P e^{-h_m/h_P}). \tag{19}$$

For a finite value of h_P, the buoyancy flux $b_* u_*$ will be decreased relative to that when h_P is infinitesimally small (equivalent to complete absorption of the heat flux at the air–sea interface), thereby implying a deeper mixed layer when subsurface heating is included in an OGCM with an embedded mixed layer. Similarly, when deepening (i.e., $P > 0$), the mixed layer will be deeper with the inclusion of subsurface heating (finite vs infinitesimal h_P) because $b_* u_*$ will become smaller and increase the amount of TKE (P) available for entraining fluid into the mixed layer.

d. Model spinup

The six-layered thermodynamic model without the mixed layer is spun up to statistical energy equilibrium and then continued for 5 years with a mixed layer and climatological forcing. Climatological monthly means of the thermal forcing are obtained from the Comprehensive Ocean–Atmosphere Data Set (COADS) (da Silva et al. 1994). Thermal forcing includes shortwave (incoming solar) plus longwave radiation (Q_R), air temperature (T_a) at 10 m, and the air mixing ratio (q_a) at 10 m. Scalar wind speed (v_a) is obtained from the input wind stress, which has 6-hourly variability. All climatological model simulations with a mixed layer are performed using climatological 6-hourly hybrid winds. These consist of monthly Hellerman and Rosenstein (1983) wind stresses (HR) plus ECMWF wind anomalies (Wallcraft et al. 2003). We add a high-frequency component to the climatological forcing because of its impact on the mixed layer and because the model is targeted at simulations forced by high-frequency interannual atmospheric fields from operational weather centers. After reaching statistical energy equilibrium, the climatological model simulation with a mixed layer is extended using interannual surface forcing from 1996 and 1997. In this case, the 6-hourly thermal forcing from ECMWF includes the shortwave plus longwave radiation (Q_R), air temperature (T_a) at 10 m, and air mixing ratio (q_a) at 10 m. None of the model simulations presented in this paper include assimilation of any SST data.
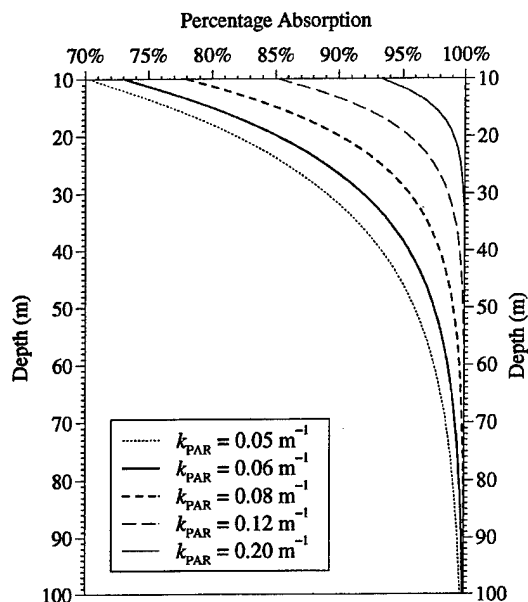
FIG. 2. Percentage absorption of solar radiation with depth (h) calculated using a single exponential decay formula. These profiles are good representatives of solar transmission in the visible band within the mixed layer below 10 m. The same approach is also used in NLOM.

3. Turbidity effects on NLOM simulations

In this section, sensitivity of model results to water turbidity is examined with a particular focus on SST and MLD simulations. The model results are then compared with daily SST and MLD time series obtained from buoys located in different regions of the global ocean.

a. Global turbidity effects

Before analyzing the model results, we first examine where turbidity might be important to the annual mean and seasonal cycle of the mixed layer. Our purpose is to indicate the regions where k_{PAR} variability can affect the SST simulation over the global ocean. The greatest interest is in those situations where subsurface heating can occur below the mixed layer, thereby resulting in a cooler SST than is obtained by assuming complete absorption of solar irradiance within the bulk mixed layer. This is expected to occur in regions of small k_{PAR} values. The reverse situation of large k_{PAR} values is expected to produce complete (or almost complete) absorption of the solar radiation within the mixed layer because a minimum MLD of 10 m is imposed by the NLOM. It is noted that, based on a single exponential approach [100−49.0 exp($-hk_{PAR}$)] as shown in Fig. 2, all large k_{PAR} values (i.e., $k_{PAR} > 0.20$ m^{-1}) are essentially uniform.

Three different k_{PAR} values are considered: 1) a monthly k_{PAR} dataset to account for the seasonal and

spatial variation of subsurface heating, 2) a global constant value of $k_{PAR} = 0.06$ m^{-1} that is representative of most open-ocean conditions, and 3) an unrealistically large value of $k_{PAR} = 99$ m^{-1} to ensure the complete absorption of solar radiation within the mixed layer. Case 2 corresponds to an e-folding penetration depth of $h_P = k_{PAR}^{-1} = 16.7$ m with 95% absorption by 50-m depth. This is close to h_P values used in other studies: 15 (Schneider and Zhu 1998), 17 (Murtugudde et al. 2002), and 23 m (Nakamoto et al. 2001). Case 3 represents traditional OGCM approaches (e.g., Yuen et al. 1992; Murtugudde et al. 1995).

For all three cases the monthly mean radiation absorbed below the mixed layer is calculated using Q_P exp($-z/h_P$), with h_P [cf. Eq. (5)] defined as a temporally interpolated monthly global field. These calculations use global climatologies of monthly k_{PAR} and monthly optimal MLD based on observations (Kara et al. 2003a). Then, the differences of cases $1 − 2$ and cases $1 − 3$ are calculated month by month and presented as a percentage relative to the net surface heat flux at the ocean surface Q_a. Note here that case $1 −$ case 2 represents the percentage difference absorbed from using monthly versus $k_{PAR} = 0.06$ m^{-1}, and case $1 −$ case 3 is just case 1 because Q_P is assumed to be zero for case 3. Last, global maps of the annual mean and the maximum value over the 12 months are formed. The reason for using a worst-month approach is the root-mean-square error (rmse) would not be a useful measure of turbidity impact because the error is likely to be near zero whenever the MLD is deep. The annual-mean climatological MLD is as shallow as 10 m in some regions where absorption is greater, such as parts of the equatorial region and the North Pacific (see KHR). This is especially evident in summer months. For example, strong solar heating occurs in conjunction with optical depths on the order of 10–15 m throughout the year in the equatorial Pacific.

The impact of a space- and time-varying k_{PAR} can be most easily determined from the ratio of PAR below the MLD relative to the PAR at the air–sea interface. An examination of the annual mean difference between experiments for this PAR fraction expressed as a percentage (Figs. 3a and 3b) reveals that k_{PAR} has essentially no effect over most of the global ocean (regions displayed as white). This occurs where PAR penetration below the MLD is low because of a relatively deep mixed layer most of the time. The relatively deep annual mean MLD, as shown in KHR, tends to correlate well with Fig. 3a and/or high turbidity, especially in relation to Fig. 3c. Using a monthly k_{PAR} makes a large difference (in at least one month) at high latitudes and in the equatorial ocean (Fig. 3c). The sensitivity to solar attenuation in the Tropics agrees with earlier studies (Murtugudde et al. 2002; Nakamoto et al. 2001; Schneider and Zhu 1998). Note that the absorption anomaly only indicates when solar heating within the mixed layer is significantly affected by turbidity and does not indicate its influence on SST.
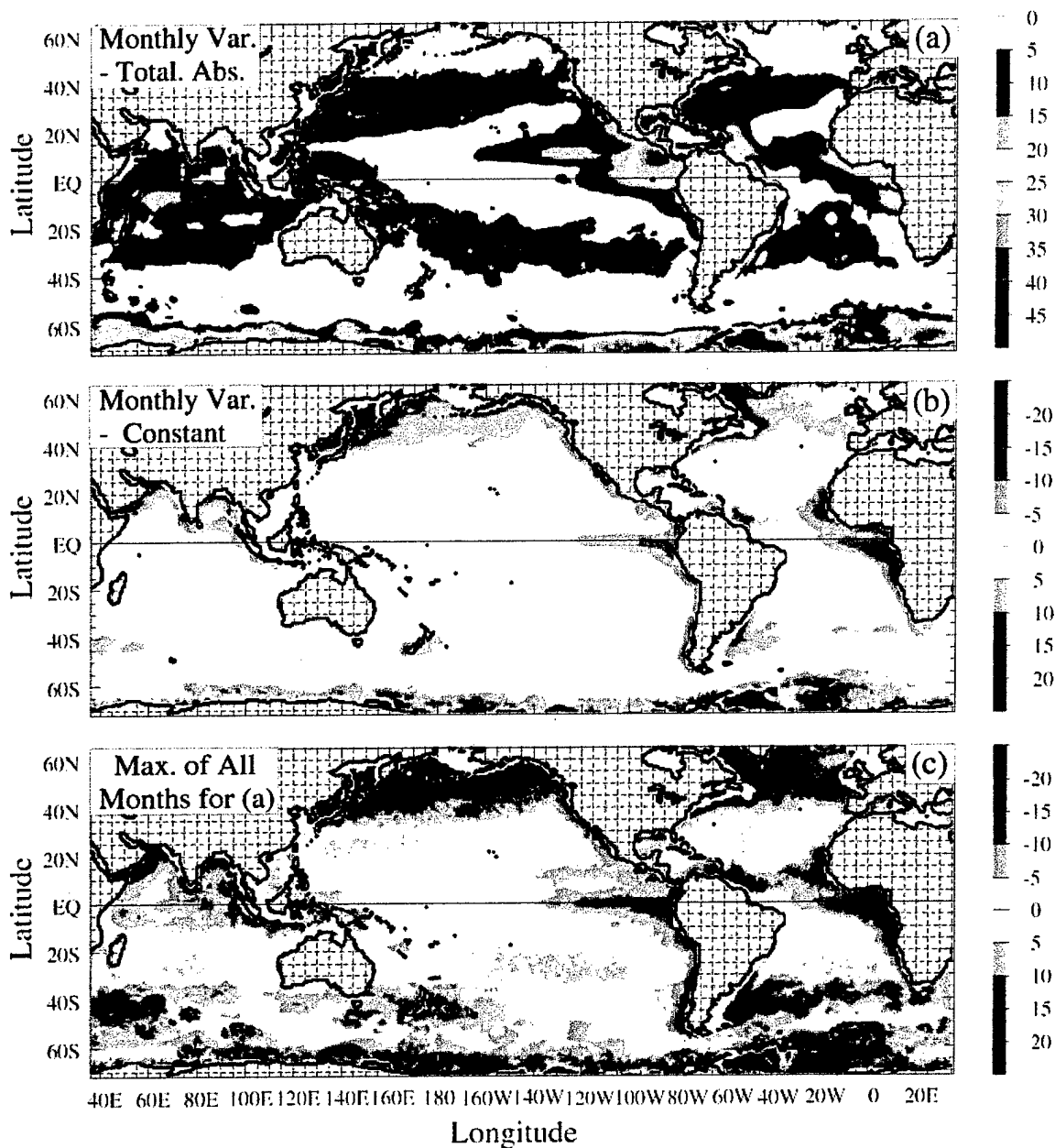
FIG. 3. Changes in PAR below the MLD as percentage of PAR at the surface: (a) annual-mean difference when using a monthly varying k_{PAR} relative to complete PAR absorption within the mixed layer (i.e., the effect of ignoring k_{PAR}), (b) annual-mean difference when using a monthly varying k_{PAR} relative to $k_{PAR} = 0.06$ m^{-1}, and (c) largest difference of all 12 months for case (b), indicating where using a monthly k_{PAR} can make a large difference in model simulations.

Based on the observational results presented above, interannual model simulations that use three different k_{PAR} values are performed to investigate the effects of ocean turbidity for the model SST and MLD simulations in 1996 and 1997 (see Table 1 for a brief explanation of each experiment performed). The model spinup and forcing were already described in section 3. For exper-

iment 1, spatially and monthly varying k_{PAR} values interpolated to the global NLOM grid are used. For experiment 2, the global ocean turbidity is set to a constant, $k_{PAR} = 0.06$ m^{-1}. In experiment 3, all of the solar radiation is absorbed in the mixed layer by using a very large k_{PAR} value. Differences between experiments 1 and 2 are only expected near the equator and in coastal

TABLE 1. The three interannual NLOM simulations for 1996 and 1997. The model has an embedded bulk-type mixed layer. It used wind and thermal forcings (i.e., air temperature at 10 m, air mixing ratio at 10 m, shortwave and longwave radiation) from the 6-hourly ECMWF data.

Expt	k_{PAR}	Description of the expt
1	Variable	Spatial and temporal turbidity
2	0.06 m^{-1}	Constant turbidity over the global ocean
3	99 m^{-1}	All solar radiation absorbed in mixed layer

regions where larger space- and time-varying k_{PAR} values occur (Fig. 3). Differences in SST between these two simulations only occur in regions where a shallow MLD coincides with a monthly varying k_{PAR} that differs substantially from 0.06 m^{-1}.

b. NLOM model–data comparisons

For model–data comparisons, the daily averaged SSTs obtained from the three interannual NLOM simulations are compared with daily averaged SST time series from moored buoys located in different regions of the global ocean. These are obtained from the Tropical Atmosphere–Ocean (TAO) array (McPhaden 1995) and the National Oceanic Data Center (NODC). In both datasets, SST is measured at a depth of 1 m below the sea surface. The model and buoy SSTs are compared using several statistical metrics (e.g., Stewart 1990; Murphy 1988) as described next. Let v_i ($i = 1, 2, \ldots, N$) be the set of N observed (i.e., buoy) SSTs, and let e_i ($i = 1, 2, \ldots, N$) be the set of NLOM SSTs. Also let $\bar{v}(\bar{e})$ and $\sigma_v(\sigma_e)$ be the mean and standard deviations of the buoy (NLOM) SSTs. The statistical measures can then be expressed as follows:

$$ME = \bar{e} - \bar{v}, \tag{20}$$

$$R = \frac{1}{n} \sum_{i=1}^{n} (v_i - \bar{v}) \frac{(e_i - \bar{e})}{(\sigma_v \sigma_e)}, \tag{21}$$

$$(rmse)^2 = \frac{1}{n} \sum_{i=1}^{n} (e_i - v_i)^2, \quad \text{and} \tag{22}$$

$$SS = 1 - \frac{(rmse)^2}{\sigma_v^2}, \tag{23}$$

where ME is the mean error, rmse is the root-mean-square difference, R is the correlation coefficient, and SS is the skill score. Because the standard deviation of SST is different for each buoy, rmse between the model and the buoy will not entirely reflect model performance. Thus, we also include a dimensionless measure (SS) that takes account of the bias between the model and buoy SST; SS = 1 for a perfect estimate (Murphy 1988). Negative SS values indicate the model SSTs do not compare well with the buoy SSTs.

Table 2 statistically compares the daily averaged NLOM SSTs from the three experiments with TAO buoy SSTs in 1997, and Table 3 shows the same for NODC buoy SSTs outside the equatorial region. Overall, the ME values are small between the NLOM and buoy SSTs for all locations. The NLOM is able to capture SST variability well because correlation coefficients are close to $R = 1$ in most of the cases. Large and positive SS values show that the NLOM is able to simulate SST with skill. This is especially true when turbidity effects (i.e., variable k_{PAR}) are taken into account (expt 1). Using a constant k_{PAR} (expt 2) rather than variable k_{PAR} did not significantly affect the results for the locations used in this study. However, we clearly see that absorption of all solar radiation into the mixed layer (expt 3) simulates the SST less accurately. This is not surprising because

TABLE 2. Statistical verification of daily SST time series between NLOM and TAO buoys at different locations in the equatorial ocean. Comparisons are made during a 1-yr period (1997). All statistical calculations are based on 365 daily SST values.

Location	Expt	Rmse (°C)	ME (°C)	σ_{BUOY} (°C)	σ_{NLOM} (°C)	R	SS
(0°, 110°W)	1	1.31	−0.26	1.45	0.99	0.50	0.18
	2	1.35	−0.38	1.45	1.02	0.50	0.14
	3	1.61	0.07	1.45	1.14	0.34	−0.23
(0°, 125°W)	1	1.21	0.05	1.64	1.06	0.68	0.46
	2	1.23	0.12	1.64	1.09	0.67	0.44
	3	1.35	0.31	1.64	1.20	0.61	0.33
(0°, 155°W)	1	0.77	−0.13	1.44	1.03	0.86	0.72
	2	0.78	−0.13	1.44	0.97	0.87	0.71
	3	0.87	0.09	1.44	1.09	0.80	0.64
(0°, 170°W)	1	0.62	−0.32	0.89	0.72	0.80	0.51
	2	0.66	−0.40	0.89	0.70	0.80	0.44
	3	0.64	−0.06	0.89	0.89	0.75	0.49
(5°N, 155°W)	1	0.55	−0.14	0.98	0.97	0.85	0.69
	2	0.53	−0.15	0.98	1.00	0.87	0.70
	3	0.61	−0.06	0.98	1.05	0.82	0.62
(8°S, 110°W)	1	0.70	−0.43	0.71	0.71	0.68	0.08
	2	0.70	−0.44	0.71	0.70	0.68	0.08
	3	0.77	−0.31	0.71	0.78	0.62	−0.17

TABLE 3. As in Table 2 but for 1996 and with statistical verification performed using NODC buoys outside the equatorial ocean.

Location	Expt	Rmse (°C)	ME (°C)	σ_{BUOY} (°C)	σ_{NLOM} (°C)	R	SS
(26°N, 94°W), Gulf of	1	0.58	−0.36	3.19	3.21	0.99	0.97
Mexico	2	0.61	−0.40	3.19	3.19	0.99	0.96
	3	0.63	−0.01	3.19	3.61	0.96	0.96
(29°N, 79°W), Florida coast	1	0.83	0.41	2.15	2.49	0.96	0.85
	2	0.80	0.38	2.15	2.47	0.96	0.86
	3	1.19	0.69	2.15	2.79	0.95	0.70
(38°N, 130°W), off southwest	1	0.97	−0.42	1.63	2.07	0.91	0.64
United States	2	0.97	−0.49	1.63	2.05	0.92	0.64
	3	1.03	−0.28	1.63	2.18	0.91	0.60
(41°N, 137°W), off northwest	1	0.67	0.08	2.94	2.99	0.97	0.95
United States	2	0.63	.03	2.94	2.97	0.98	0.95
	3	0.99	0.32	2.94	3.29	0.96	0.89
(46°N, 131°W), off northwest	1	0.83	−0.01	2.85	3.09	0.96	0.91
United States	2	0.77	−0.08	2.85	3.04	0.97	0.93
	3	1.03	0.15	2.85	3.29	0.96	0.87
(52°N, 156°W), Alaska coast	1	0.78	0.41	2.66	2.87	0.97	0.91
	2	0.67	0.33	2.66	2.77	0.98	0.94
	3	0.82	0.43	2.66	2.89	0.97	0.91

this choice can affect SST in two ways: 1) by allowing too much solar radiation to be absorbed in the mixed layer and 2) by influencing the stability of the upper ocean and thus SST.

To further examine the effects of turbidity the observed SSTs from two moorings are compared with those obtained from the three NLOM experiments (Fig. 4): one located in the central equatorial Pacific (0°,
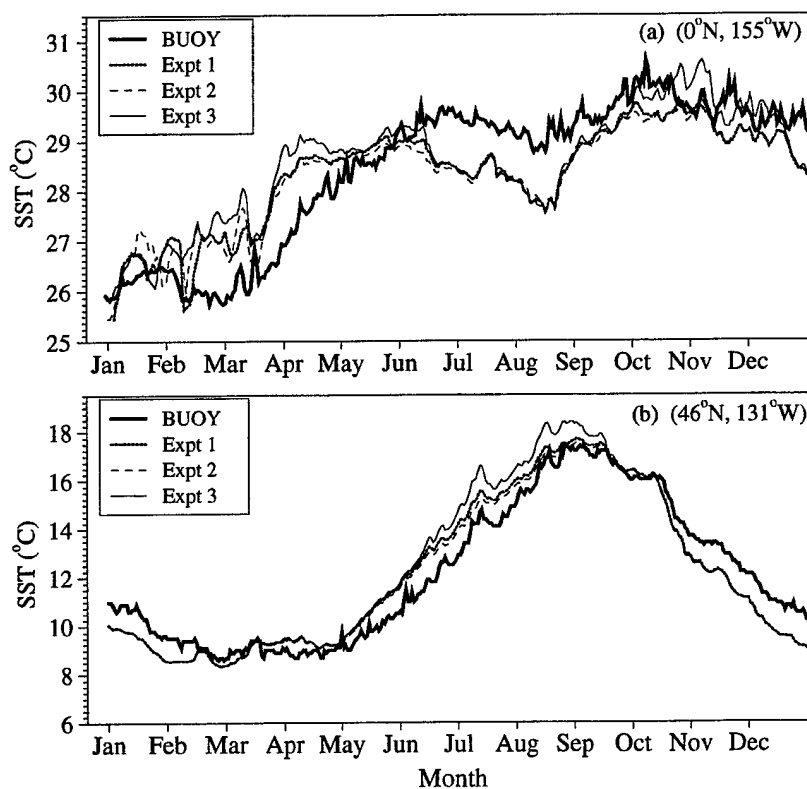

FIG. 4. Daily averaged SST time series comparisons between two buoys and three NLOM experiments (see Table 1). Two different buoy locations are used in two different years: (a) equatorial ocean (0°, 155°W) in 1997 and (b) off the northwest coast of the United States (46°N, 131°W) in 1996. See Fig. 5 for monthly k_{PAR} values at these locations.
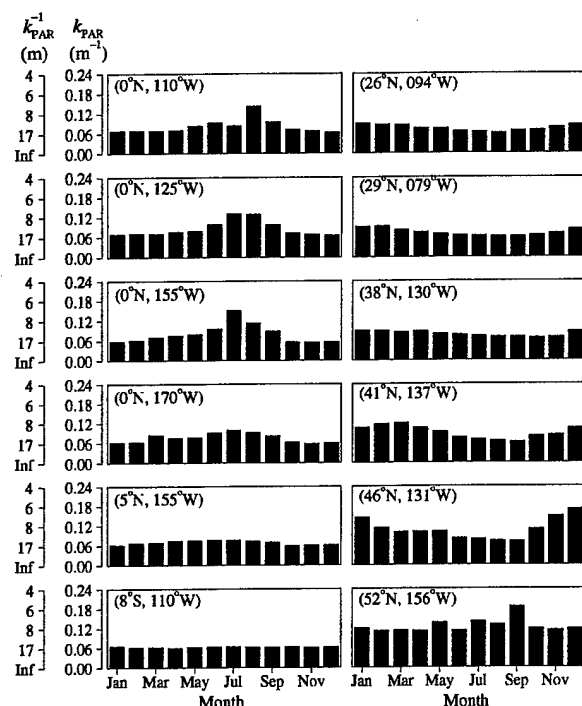
FIG. 5. Climatological monthly mean of k_{PAR} at the locations given in Tables 2 and 3. Note that x-axis labels are written for every other month.

155°W), and the other off the U.S. northwest coast (46°N, 131°W). Recall that experiment 1 is performed using turbidity at each buoy location as represented by the monthly SeaWiFS k_{PAR} values. For the buoy at (0°, 155°W), it is obvious that complete absorption of solar radiation within the mixed layer (expt 3) produces the highest SST from February through April and from October through November. Note that k_{PAR} values at this location are greater than 0.06 m^{-1} for February–April but not October–November (Fig. 5). Clearly, absorption of all solar radiation (expt 3) in the mixed layer causes a relatively large warm bias between the NLOM SST and buoy SST at this location. A similar warm bias was found in the annual mean SST by Schneider and Zhu (1998) between simulations assuming no solar penetration and a constant attenuation depth for solar penetration. As for (46°N, 131°W), the SST differences between experiment 1 (the standard simulation) and experiment 2 are again small. These results agree with other studies (e.g., Murtugudde et al. 2002) that find larger SST changes occurring at low latitudes. Experiment 3 produces the highest SST, and the difference with respect to experiments 1 and 2 is largest for June–September.

To determine how the differences between the SST simulations may be due to differences in MLD, we used daily averaged subsurface temperature measurements from (0°, 155°W) to determine the daily MLD. Subsurface parameters from the buoys include daily water

temperatures at 10 discrete depths between 25 and 500 m. For this buoy they are 25, 50, 75, 100, 125, 150, 200, 250, 300, and 500 m. Subsurface temperature accuracy is about 0.01°–0.05°C for the different sensors used (Freitag et al. 1994). Salinity measurements from the buoys were not available for the location. Thus, an isothermal layer depth (ILD) definition is used with a ΔT value of 0.5°C. The ILD can be summarized in its simplest form as being the depth at the base of an isothermal layer where the temperature has changed by a fixed amount of $\Delta T = 0.5°C$ from the temperature at a reference depth of 10 m. A layer depth obtained using the ILD with this ΔT value is approximately equal to true mixed MLD in the equatorial ocean (Kara et al. 2000c). Figure 6 shows the daily buoy MLD as well as those from the three NLOM simulations. There are very small differences in MLDs from the three experiments.

Overall the model MLD is shallow. As expected based on turbulence considerations (cf. section 3c), the MLD in general deepened when subsurface heating was permitted within the OGCM. However, the changes at this particular location were not significant. For example, the ME values between the buoy MLD and those obtained from the three experiments are close to each other with values of -15.1, -14.8, and -14.8 m, respectively. Large SST differences do not occur during winter at (46°N, 131°W) because of the deep MLD (not shown). When heat storage is distributed over a thicker ocean layer, the amplitude of the SST variations decreases (Schneider and Zhu 1998). Since subsurface temperatures were unavailable for this buoy, a monthly MLD climatology (Kara et al. 2003a) based on temperature and salinity profiles from the *World Ocean Atlas 1994* (Levitus et al. 1994; Levitus and Boyer 1994) was used as a proxy for the observed MLD. The MLD climatology has been previously shown to be in good agreement with hydrographic profiles taken at (49°N, 131°W) giving confidence in its use as a proxy for the mooring at (46°N, 131°W).

To investigate NLOM performance in predicting MLD we used a normalized rmse defined as

$$(\text{nrmse})^2 = \frac{1}{n} \sum_{i=1}^{n} \left[\frac{(e_i - v_i)}{v_i} \right]^2,$$

where v_i ($i = 1, 2, \ldots, n$) is the set of N buoy values and e_i ($i = 1, 2, \ldots, n$) is the set of estimates from the NLOM. The nrmse is used because the MLD amplitude error tends to be proportional to MLD and use of a fractional MLD error prevents the larger errors that occur when the MLD is deep from dominating the error assessment. The nrmse values between the buoy MLD and the three experiments are almost identical with values of 0.33, 0.34, and 0.33. These nrmse values show the errors for the NLOM estimates are approximately 33% of the buoy MLDs. Previously Kantha and Clayson (1994) pointed out the influence on the mixed layer of upwelling and downwelling processes that are so prev-

Month

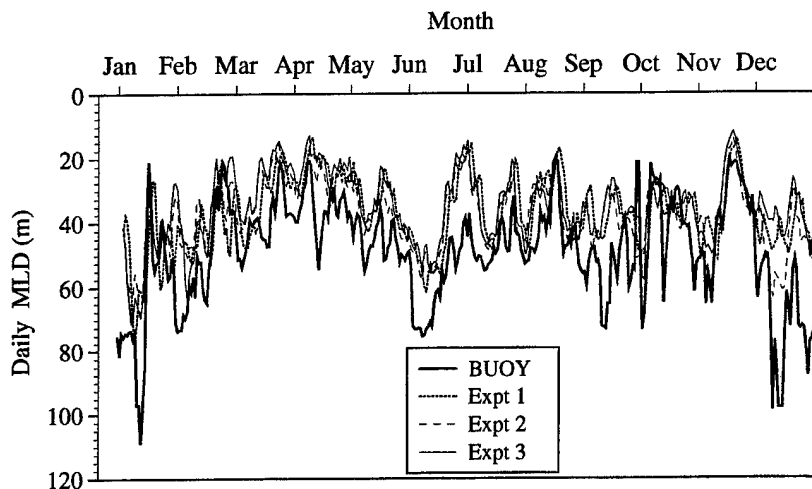Jan Feb Mar Apr May Jun Jul Aug Sep Oct Nov Dec

FIG. 6. Daily averaged MLD time series comparisons between values calculated from buoy subsurface temperatures and those from the three NLOM experiments at (0°, 155°W) in 1997. See Fig. 5 for monthly k_{PAR} values at this location.

alent at the equator, making MLD simulation from a bulk or diffusion model difficult. Taking this into consideration, we can nevertheless state that the NLOM is still able to predict MLD well with an annual-mean error of only ~15 m.

It is noted that experiments 1 and 2 produce an SST that differs only slightly in the annual mean despite the strong monthly k_{PAR} variation used in experiment 1. This very small change in the annual mean SST can be most easily explained by examining the compensation depth

Month

Jan Feb Mar Apr May Jun Jul Aug Sep Oct Nov Dec

FIG. 7. Compensation depths computed from k_{PAR} for the two mooring locations shown in Fig. 4. Also shown are daily time series of model MLD from experiment 1.

(D_C). The latter is defined as the depth at which the PAR decreases to 1%,

$$D_C = \frac{\ln(0.01)}{k_{PAR}}, \qquad (24)$$

and is routinely used in ocean biology (Lalli and Parsons 1997). In the present context D_C represents the maximum depth for solar heating of the upper ocean. The maximum value of D_C that occurs during the year represents the full extent of the water column over which thermal energy from solar heating is stored. Whenever the MLD attains or exceeds the maximum D_C value for the seasonal cycle, the thermal energy from solar heating that was not absorbed in the mixed layer because of penetration below the mixed layer during the remainder of the year is entirely entrained into the mixed layer. Figure 7 shows the compensation depth computed from the monthly k_{PAR} values and the MLD from experiment 1 at the two mooring locations shown in Fig. 4. At both locations the model MLD in January deepens to almost, or beyond, the maximum value. The same annual integrated heating is therefore obtained in experiments 1 and 2 because the mixed layer entrains all of the solar heating input into the upper ocean over the seasonal cycle. In other words, the mixed layer allows the experiment with space- and time-varying k_{PAR} to achieve nearly the same annual integrated heating as the experiment with constant $k_{PAR} = 0.06$ m^{-1}. Ohlmann et al. (1996) previously identified this mechanism when they pointed out that penetrating solar energy can be trapped within the seasonal pycnocline at mid- and high latitudes, with this thermal energy becoming unavailable for exchange with the atmosphere until winter mixed layer deepening.
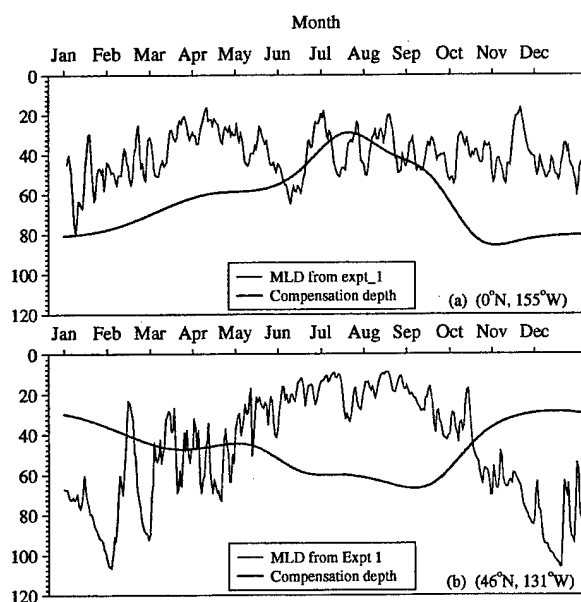
c. Comparisons with other OGCM studies

With regard to other studies, we note here that Murtugudde et al. (2002) report annual-mean SST differences as large as $-0.5°C$ between their variable and constant-attenuation-depth simulations in the Tropics by using a primitive equation OGCM that has 19 sigma layers beneath a surface mixed layer. They found that warming of the water column below the mixed layer led to an SST warming in the Tropics despite penetrating solar radiation below the mixed layer. In contrast, we find the SST decreases when permitting penetration of solar radiation. These different outcomes are likely due to the different data sources and methods used for calculating the penetration of solar radiation. Murtugudde et al. (2002) obtain penetration depths from the CZCS data that are from 10–20 m greater than those obtained here using the SeaWiFS data. The larger penetration depths lead to solar heating being distributed over a greater depth of the upper ocean, thereby producing a weaker and deeper thermocline. As a consequence, wind-deepening events more easily erode the thermocline than when solar penetration is neglected. This leads to larger amounts of appreciably warmer water being entrained into the mixed layer and, thus, a warmer SST and deeper MLD. The lesser penetration depths used in this study result in a stronger and shallower thermocline. This permits colder water to be entrained during wind-deepening events and sustains a shallower mixed layer. This combines to produce an SST that is colder than when solar penetration is neglected. The opposing results from these two studies point to the sensitivity of SST in the Tropics to the parameterization of the penetration depths.

Earlier studies consistently find much larger differences in the mean MLD error between simulations performed when excluding and including sunlight penetration below the ocean surface than those reported here. For example, using a Richardson-number-dependent vertical mixing scheme of heat and momentum, Schneider and Zhu (1998) found mean MLD errors increased by 30 m off the equator in the Pacific, while the mean MLD error increased by 10–30 m at the equator. Murtugudde et al. (2002) obtained annual-mean MLD differences of up to 12 m between their variable and constant-attenuation-depth simulations in the Tropics. This is a threefold increase over the annual mean MLD difference of 2–4 m that we obtained between our corresponding simulations. Nakamoto et al. (2001) report mean MLD errors of 20–40 m in the western and central equatorial Pacific. These larger differences relative to our findings can be related to the greater penetration depths obtained using the CZCS versus SeaWiFS data. The greater depth penetration obtained from the CZCS data permits a larger value for the radiation contribution B_{rad} in the ATKE equation [see Eq. (7)] and thus a deeper MLD.

Kantha and Clayson (1994) performed a one-dimen-

sional ocean model study to examine turbidity effects on SST. The model was based on second-order closure of turbulence. They noted that the SST rise for a very shallow MLD is highly sensitive to the parameterization of solar extinction. However, their results were limited because they used the Secchi depth approach (Gordon and Wouters 1978) to determine ocean turbidity in the simulations and used it for only one location. They concluded that there could be as large as 1°C differences in SST when using different turbidity in model simulations. This is confirmed by the variety of buoys used in this study. Results presented in this paper support the conclusion of Kantha and Clayson (1994) that, if available, a model simulation should include turbidity to account for variations in solar radiation extinction in the mixed layer. However, a constant turbidity (i.e., $k_{PAR} = 0.06 \text{ m}^{-1}$) assumption is also adequate to obtain reliable SSTs in global ocean simulations. Although there can be differences in SST for some months when using a variable ocean turbidity rather than using constant k_{PAR}, overall there are no significant differences between SSTs obtained from experiment 1 and experiment 2 over annual time scales. This is true for the two buoy locations that we examined in detail and statistically for a large number of buoys (see Tables 2 and 3). Assuming a constant $k_{PAR} = 0.06 \text{ m}^{-1}$ instead of using a spatially and temporally varying k_{PAR} does not change the SST simulation very much.

4. Summary and conclusions

In this paper, the impact of solar subsurface heating using space- and time-varying turbidity on SST and MLD simulations have been examined using the global Naval Research Laboratory Layered Ocean Model with an embedded bulk-type mixed layer model. The model used 6-hourly wind and thermal forcings from the European Centre for Medium-Range Weather Forecasts during 1996 and 1997. However, it develops its own sensible and latent heat fluxes from this forcing input and model SST. In the model, the attenuation of solar radiation with depth was included by using a global monthly attenuation of photosynthetically available radiation, denoted as k_{PAR}, climatology. These global fields of k_{PAR} are derived from the Sea-Viewing Wide Field-of-View Sensor data on the spectral diffuse attenuation coefficient at 490 nm (k_{490}). This study showed that differences in SST and MLD values simulated using a spatially and temporally varying attenuation parameter versus a constant attenuation value of 0.06 m^{-1} were small when averaged over the course of a year but were significant on shorter time scales.

To determine the impacts of ocean turbidity on SST simulations and find an indication of where to use a monthly k_{PAR} climatology over the global ocean, the percentage of PAR absorbed below the mixed layer was calculated using global monthly mixed layer depth (MLD) and k_{PAR} climatologies. In addition, three dif-

ferent ocean model experiments were used. The first experiment used a spatially and temporally varying global monthly k_{PAR} climatology, the second experiment used a constant k_{PAR} value of 0.06 m^{-1}, and the last experiment assumed all radiation was completely absorbed within the mixed layer. For the present application, the greatest interest is in two situations: 1) where subsurface heating occurs below the mixed layer (Fig. 3), thereby resulting in a cooler SST than obtained by assuming complete absorption of solar irradiance within the ocean general circulation model (OGCM) mixed layer (expts 1 and 2 vs expt 3) or 2) where sub–mixed layer heating is substantially reduced by high turbidity (expt 1 vs expt 2). Comparisons of daily SSTs obtained from the three NLOM simulations with buoy SSTs showed that using monthly varying water type rather than using the constant k_{PAR} approach in all months usually yields the best SST simulation from the model at low latitudes. The SST differences can vary from one month to another depending on k_{PAR} and are larger when the k_{PAR} value is large. However, considering one year-long daily SST time series, statistical analysis revealed that the differences between experiments 1 and 2 are small, at least for the buoy locations examined here. It was also found that allowing absorption of all solar radiation entering the mixed layer (expt 3) yields degraded SST simulations.

Last, we have also shown the sensitivity of a six-layer OGCM to water turbidity and compared it with other studies using OGCMs with different vertical resolutions and physical parameterizations: a coupled atmosphere–ocean general circulation model and a reduced-gravity, primitive equation OGCM having 19 sigma layers beneath a surface mixed layer. As noted, the effects of water turbidity on SST and MLD prediction can vary substantially when using different types of OGCMs because of differences in physical parameterization, forcing, and turbidity product used.

APPENDIX

List of Symbols

$b_* w_*$	Buoyancy (m^2 s^{-3})
B_{rad}	Contribution due to attenuation of solar radiation (W m^{-2})
C_{pa}	Specific heat of air (1004.5 J kg^{-1} K^{-1})
C_{pw}	Specific heat of water (3993 J kg^{-1} K^{-1})
D_C	Maximum depth of solar heating of the upper ocean
$\bar{e}$	Mean of NLOM SST time series (°C)
f^+	Coriolis parameter at 5° latitude (2.5 × 10^{-5} s^{-1})
h_m	Mixed layer depth (m)
h_m^+	Minimum mixed layer depth (10 m)
h_m^*	Mixed layer equilibrium depth (m)
h_P	Radiation absorption e-folding length scale (m)
k_{490}	Diffusive attenuation coefficient at 490 nm (m^{-1})
k_{PAR}	Attenuation coefficient for photosynthetically available radiation (m^{-1})
K_H	Coefficient of horizontal temperature diffusivity (0 m^2 s^{-1})
m_i	Kraus–Turner constants ($m_1 = 6.25$, $m_3 = 7.5$, $m_5 = 6.3$, $m_6 = 0.3$)
ME	Mean error (°C)
n_c	Kraus–Turner constant ($n_c = 1$)
N	Number of cases in the time series
nrmse	Normalized root-mean-square difference
P	Net rate of ATKE generation (m^3 s^{-3})
PAR	Photosynthetically available radiation (W m^{-2})
Q_a	Net heat flux at the ocean surface (W m^{-2})
Q_{IR}	Infrared radiation (W m^{-2})
Q_L	Latent heat flux (W m^{-2})
Q_{LW}	Net longwave radiation at sea surface (W m^{-2})
$Q_P(z)$	Penetrating solar radiation at depth z (W m^{-2})
Q_S	Sensible heat flux (W m^{-2})
Q_{SOL}	Solar irradiance at the sea surface (W m^{-2})
$Q(z)$	Net surface heat flux at depth z (W m^{-2})
R	Linear correlation coefficient
rmse	Root-mean-square difference (°C)
SS	Skill score
t	Time (s)

T_b	Temperature just below the mixed layer (°C)
T_m	Sea surface temperature (°C)
u_*	Friction velocity (m s^{-1})
$\mathbf{v}_1$	Layer-1 velocity (m s^{-1})
$\alpha(T_m)$	Coefficient of thermal expansion of seawater (°C^{-1})
ΔT_b	Temperature shear (°C)
ΔT_b^+	Minimum temperature difference (0.2°C)
ΔT_m	Temperature change across the mixed layer (°C)
ω_m	Vertical mixing velocity (m s^{-1})
Ω	Rotation rate of the earth (7.292 $\times$ 10^{-5} s^{-1})
ϕ	Latitude (°)
ρ_0	Reference density for seawater (1000 kg m^{-3})
σ_e	Standard deviation of NLOM SST time series (°C)
σ_v	Standard deviation of buoy SST time series (°C)
σ_ω^{-1}	MLD relaxation e-folding time (s)
$\bar{v}$	Mean of buoy SST time series (°C)
τ_a	Wind stress (N m^{-2})

REFERENCES

Austin, R. W., and T. J. Petzold, 1986: Spectral dependence of the diffuse attenuation coefficient of light in ocean waters. *Opt. Eng.*, **25**, 471–479.

Brock, J. S., and J. S. McClain, 1992: Interannual variability in phytoplankton blooms observed in the northwestern Arabian Sea during the southwest monsoon. *J. Geophys. Res.*, **97**, 733–750.

——, S. Sathyendranath, and T. Platt, 1993: Modeling the seasonality of submarine light and primary production in the Arabian Sea. *Mar. Ecol. Prog. Ser.*, **101**, 209–221.

da Silva, A. M., C. C. Young, and S. Levitus, 1994: *Algorithms and Procedures.* Vol. 1, *Atlas of Surface Marine Data*, NOAA Atlas NESDIS 6, 83 pp.

Dickey, T. D., 1983: The influence of optical water type on the diurnal response of the upper ocean. *Tellus*, **35**, 142–154.

ECMWF, 1995: User guide to ECMWF products. ECMWF Meteorological Bulletin M3.2, 71 pp. [Available from ECMWF, Shinfield Park, Reading RG2 9AX, United Kingdom.]

Freitag, H. P., Y. Feng, L. J. Mangum, M. J. McPhaden, J. Neander, and L. D. Stratton, 1994: Calibration, procedures and instrumental accuracy estimates of TAO temperature, relative humidity and radiation measurements. NOAA Tech. Memo. ERL PMEL-104, 32 pp. [Available from PMEL, 7600 Sand Point Way, Seattle, WA 98115.]

Frouin, R., D. W. Lingner, C. Gautier, K. S. Baker, and R. C. Smith, 1989: A simple analytical formula to compute clear sky total and photosynthetically available solar irradiance at the ocean surface. *J. Geophys. Res.*, **94**, 9731–9742.

Gallimore, R. G., and D. D. Houghton, 1987: Approximation of ocean heat storage by ocean–atmosphere energy exchange: Implications for seasonal cycle mixed layer ocean formulations. *J. Phys. Oceanogr.*, **17**, 1214–1231.

Garwood, R. W., 1977: An oceanic mixed layer model capable of simulating cyclic states. *J. Phys. Oceanogr.*, **7**, 455–468.

Gibson, J. K., P. Kållberg, S. Uppala, A. Hernandez, A. Nomura, and E. Serrano, 1997: ERA description. ECMWF Re-Analysis Proj-

ect Rep. Series, No. 1, 72 pp. [Available from ECMWF, Shinfield Park, Reading RG2 9AX, United Kingdom.]

Gordon, H. R., and A. W. Wouters, 1978: Some relationships between Secchi depth and inherent optical properties of natural waters. *Appl. Opt.*, **17**, 3341–3343.

Hellerman, S., and M. Rosenstein, 1983: Normal monthly wind stress over the World Ocean with error estimates. *J. Phys. Oceanogr.*, **13**, 1093–1104.

Hurlburt, H. E., and J. D. Thompson, 1980: A numerical study of Loop Current intrusions and eddy shedding. *J. Phys. Oceanogr.*, **10**, 1611–1651.

——, A. J. Wallcraft, W. J. Schmitz Jr., P. J. Hogan, and E. J. Metzger, 1996: Dynamics of the Kuroshio/Oyashio current system using eddy-resolving models of the North Pacific Ocean. *J. Geophys. Res.*, **101**, 941–976.

Jerlov, N. G., 1976: *Marine Optics.* Elsevier Oceanography Series, Vol. 14, Elsevier, 231 pp.

——, 1977: Classification of seawaters in terms of quanta irradiance. *J. Cons. Int. Explor. Mer.*, **37**, 281–287.

Kantha, L. H., and C. A. Clayson, 1994: An improved mixed layer model for geophysical applications. *J. Geophys. Res.*, **99**, 25 235–25 266.

Kara, A. B., P. A. Rochford, and H. E. Hurlburt, 2000a: An optimal definition for ocean mixed layer depth. *J. Geophys. Res.*, **105**, 16 803–16 821.

——, ——, and ——, 2000b: Efficient and accurate bulk parameterizations of air–sea fluxes for use in general circulation models. *J. Atmos. Oceanic Technol.*, **17**, 1421–1438.

——, ——, and ——, 2000c: Mixed layer depth variability and barrier layer formation over the North Pacific Ocean. *J. Geophys. Res.*, **105**, 16 783–16 801.

——, ——, and ——, 2002a: Air–sea flux estimates and the 1997–1998 ENSO event. *Bound.-Layer Meteor.*, **103**, 439–458.

——, ——, and ——, 2002b: Naval Research Laboratory mixed layer depth (NMLD) climatologies. NRL Rep. NRL/FR/7330/02/9995, 26 pp. [Available from NRL, Code 7323, Bldg. 1009, Stennis Space Center, MS 39529-5004.]

——, ——, and ——, 2003a: Mixed layer depth variability over the global ocean. *J. Geophys. Res.*, **108**, 3079, doi:10.1029/2000JC000736.

——, A. J. Wallcraft, and H. E. Hurlburt, 2003b: Climatological SST and MLD predictions from a global layered ocean model with an embedded mixed layer. *J. Atmos. Oceanic Technol.*, **20**, 1616–1632.

Kraus, E. B., and J. S. Turner, 1967: A one-dimensional model of seasonal thermocline. II. The general theory and its consequences. *Tellus*, **19**, 98–106.

Lalli, C. M., and T. R. Parsons, 1997: *Biological Oceanography: An Introduction.* Butterworth–Heinemann, 314 pp.

Le Treut, H., J. Y. Simonot, and M. Crepon, 1985: A model for the sea surface temperature and heat content in the North Atlantic Ocean. *Coupled Ocean–Atmosphere Models*, J. Nihoul, Ed., Elsevier, 439–445.

Lewis, M. R., M. E. Carr, G. Feldman, C. McClain, and W. Esaias, 1990: Influence of penetrating radiation on the heat budget of the equatorial Pacific Ocean. *Nature*, **347**, 543–545.

Levitus, S., and T. P. Boyer, 1994: *Temperature.* Vol. 4, *World Ocean Atlas 1994*, NOAA Atlas NESDIS 4, 117 pp.

——, R. Burgett, and T. P. Boyer, 1994: *Salinity.* Vol. 3, *World Ocean Atlas 1994*, NOAA Atlas NESDIS 3, 99 pp.

Lin, S.-J., W. C. Chao, Y. C. Sud, and G. K. Walker, 1994: A class of the van Leer-type transport schemes and its application to the moisture transport in a general circulation model. *Mon. Wea. Rev.*, **122**, 1575–1593.

Liu, W. T., A. Zhang, and J. K. B. Bishop, 1994: Evaporation and solar irradiance as regulators of sea surface temperature in annual and interannual changes. *J. Geophys. Res.*, **99**, 12 623–12 637.

Martin, P., 1985: Simulation of the mixed layer at OWS November and Papa with several models. *J. Geophys. Res.*, **90**, 903–916.

McClain, C. R., M. L. Cleave, G. C. Feldman, W. W. Gregg, S. B.

Hooker, and N. Kuring, 1998: Science quality SeaWiFS data for global biosphere research. *Sea Technol.,* **39,** 10–16.

McPhaden, M. J., 1995: The Tropical Atmosphere Ocean (TAO) array is completed. *Bull. Amer. Meteor. Soc.,* **76,** 739–741.

Mellor, G. L., and T. Yamada, 1982: Development of a turbulence closure model for geophysical fluid problems. *Rev. Geophys. Space Phys.,* **20,** 851–875.

Metzger, E. J., and H. E. Hurlburt, 2001: The nondeterministic nature of Kuroshio penetration and eddy shedding in the South China Sea. *J. Phys. Oceanogr.,* **31,** 1712–1732; Corrigendum, **31,** 2807.

Moore, D. R., and A. J. Wallcraft, 1998: Formulation of the NRL Layered Ocean Model in spherical coordinates. NRL Rep. NRL/ CR/7323-96-0005, 24 pp. [Available from NRL, Code 7323, Bldg. 1009, Stennis Space Center, MS 39529-5004.]

Morel, A., and D. Antoine, 1994: Heating rate within the upper ocean in relation to its bio–optical state. *J. Phys. Oceanogr.,* **24,** 1652–1665.

——, and S. Maritorena, 2001: Bio-optical properties of oceanic waters: A reappraisal. *J. Geophys. Res.,* **106,** 7163–7180.

Murphy, A. H., 1988: Skill scores based on the mean square error and their relationships to the correlation coefficient. *Mon. Wea. Rev.,* **116,** 2417–2424.

Murtugudde, R., M. Cane, and V. Prasad, 1995: A reduced-gravity, primitive equation, isopycnal ocean GCM: Formulation and simulations. *Mon. Wea. Rev.,* **123,** 2864–2887.

——, J. Beauchamp, C. R. McClain, M. R. Lewis, and A. Busalacchi, 2002: Effects of penetrative radiation on the upper tropical ocean circulation. *J. Climate,* **15,** 470–486.

Nakamoto, S., S. P. Kumar, J. M. Oberhuber, K. Muneyama, and R. Frouin, 2000: Chlorophyll modulation of sea surface temperature in the Arabian Sea in a mixed-layer isopycnal general circulation model. *Geophys. Res. Lett.,* **27,** 747–750.

——, ——, ——, J. Ishizaka, K. Muneyama, and R. Frouin, 2001: Response of the equatorial Pacific to chlorophyll pigment in a mixed layer isopycnal ocean general circulation model. *Geophys. Res. Lett.,* **28,** 2021–2024.

Niiler, P. P., and E. B. Kraus, 1977: One-dimensional models of the upper ocean. *Modeling and Prediction of the Upper Layers of the Ocean,* E. B. Kraus, Ed., Pergamon Press, 143–172.

Ohlmann, J. C., D. A. Siegel, and C. Gautier, 1996: Ocean mixed layer radiant heating and solar penetration: A global analysis. *J. Climate,* **9,** 2265–2280.

Paulson, C. A., and J. J. Simpson, 1977: Irradiance measurements in the upper ocean. *J. Phys. Oceanogr.,* **7,** 952–956.

Price, J. F., R. A. Weller, and R. Pinkel, 1986: Diurnal cycling: Observations and models of the upper ocean response to diurnal

heating, cooling and wind mixing. *J. Geophys. Res.,* **91,** 8411–8427.

Rochford, P. A., A. B. Kara, A. J. Wallcraft, and R. A. Arnone, 2001: Importance of solar subsurface heating in ocean general circulation models. *J. Geophys. Res.,* **106,** 30 923–30 938.

Schneider, E. K., and Z. Zhu, 1998: Sensitivity of the simulated annual cycle of sea surface temperature in the equatorial Pacific to sunlight penetration. *J. Climate,* **11,** 1933–1950.

Schopf, P. S., and A. Loughe, 1995: A reduced-gravity isopycnal ocean model: Hindcasts of El Niño. *Mon. Wea. Rev.,* **123,** 2839–2863.

Simonot, J.-Y., and H. Le Treut, 1986: A climatological field of mean optical properties of the World Ocean. *J. Geophys. Res.,* **91,** 6642–6646.

Simpson, J. J., and T. D. Dickey, 1981: Alternative parameterizations of downward solar irradiance and their dynamical significance. *J. Phys. Oceanogr.,* **11,** 876–882.

Smith, S. D., C. W. Fairall, G. L. Geernaert, and L. Hasse, 1996: Air–sea fluxes: 25 years of progress. *Bound.-Layer Meteor.,* **78,** 247–290.

Sterl, A., and A. Kattenberg, 1994: Embedding a mixed layer model into an ocean general circulation model of the Atlantic: The importance of surface mixing for heat flux and temperature. *J. Geophys. Res.,* **99,** 14 139–14 157.

Stewart, T. R., 1990: A decomposition of the correlation coefficient and its use in analyzing forecasting skill. *Wea. Forecasting,* **5,** 661–666.

Wallcraft, A. J., 1991: The Navy Layered Ocean Model users guide. NOARL Tech. Rep. 35, 21 pp. [Available from NRL, Code 7323, Bldg. 1009, Stennis Space Center, MS 39529-5004.]

——, and D. R. Moore, 1997: The NRL Layered Ocean Model. *Parallel Comput.,* **23,** 2227–2242.

——, A. B. Kara, H. E. Hurlburt, and P. A. Rochford, 2003: The NRL Layered Global Ocean Model (NLOM) with an embedded mixed layer submodel: Formulation and tuning. *J. Atmos. Oceanic Technol.,* **20,** 1601–1615.

Woods, J. D., 1994: The upper ocean and air–sea interaction in global climate. *The Global Climate,* J. J. Houghton, Ed., Cambridge University Press, 141–178.

——, W. Barkman, and A. Horch, 1984: Solar heating of the oceans, diurnal, seasonal and meridional variation. *Quart. J. Roy. Meteor. Soc.,* **110,** 633–656.

Yuen, C. W., J. Y. Cherniawsky, C. A. Lin, and L. A. Mysak, 1992: An upper ocean general circulation model for climate studies: Global simulation with seasonal cycle. *Climate Dyn.,* **7,** 1–18.

Zaneveld, J. R. V., and R. W. Spinrad, 1980: An arctangent model of irradiance in the sea. *J. Geophys. Res.,* **85,** 4919–4922.